Neuropharmacology 105 (2016) 47–60

Contents lists available at ScienceDirect

Neuropharmacology

journal homepage: www.elsevier.com/locate/neuropharm

(II) Physiological profiling of an endogenous peptide in the basal forebrain: Age-related bioactivity and blockade with a novel modulator

Antoine-Scott Badin*, Paul Morrill, Ian M. Devonshire, Susan A. Greenfield

Neuro-Bio Ltd, Building F5, Culham Science Centre, Oxfordshire, OX14 3DB, United Kingdom

ARTICLE INFO

Article history:
Received 9 October 2015
Accepted 6 January 2016
Available online 7 January 2016

Keywords:
Acetylcholinesterase
Voltage-sensitive dye imaging
Optical imaging
Electrophysiology
Field potentials
AChE-peptides
Basal forebrain
Neuronal assemblies
In vitro
Population activity

ABSTRACT

Previous studies have suggested that neurodegeneration is an aberrant form of development, mediated by a novel peptide from the C-terminus of acetylcholinesterase (AChE). Using voltage-sensitive dye imaging we have investigated the effects of a synthetic version of this peptide in the *in vitro* rat basal forebrain, a key site of degeneration in Alzheimer's disease. The brain slice preparation enables direct visualisation in real-time of sub-second meso-scale neuronal coalitions ('Neuronal Assemblies') that serve as a powerful index of brain functional activity. Here we show that (1) assemblies are site-specific in their activity profile with the cortex displaying a significantly more extensive network activity than the sub-cortical basal forebrain; (2) there is an age-dependency, in both cortical and sub-cortical sites, with the younger brain (p14 rats) exhibiting more conspicuous assemblies over space and time compared to their older counterparts (p35-40 rats). (3) AChE-derived peptide significantly modulates the dynamics of neuronal assemblies in the basal forebrain of the p14 rat with the degree of modulation negatively correlated with age, (4) the differential in assembly size with age parallels the level of endogenous peptide in the brain, which also declines with maturity, and (5) this effect is completely reversed by a cyclised variant of AChE-peptide, 'NBP14'. These observations are attributed to an enhanced calcium entry that, according to developmental stage, could be either trophic or toxic, and as such may provide insight into the basic neurodegenerative process as well as an eventual therapeutic intervention.

1. Introduction

A peptide derived from the C-terminus of acetylcholinesterase (AChE) has a bioactivity independent of cholinergic transmission: it enhances calcium entry via an allosteric site on alpha-7 acetylcholine receptors (α_7-nAChR) (Greenfield, 2013), which in turn results in trophic-toxic effects in organotypic cell cultures (Day and Greenfield, 2004) and neuronal cell lines (Garcia-Rates et al., 2013), longer term proliferation of α_7-nAChRs (Bond et al., 2009), and enhancement of calcium potentials in mammalian brain slices (Bon and Greenfield, 2003), leading to enhanced long-term potentiation (Greenfield et al., 2004). Moreover, the trophic action of AChE-peptide can also be observed at the more complex level of 'meso-scale' brain operations, where it modulates sub-second, large-scale neuronal coalitions ('neuronal assemblies') (Gerstein et al., 1989) in the cortex via α_7-nAChRs (Badin et al., 2013), thereby having an eventual effect on plasticity via calcium influx (Broide and Leslie, 1999).

One suggestion for the underlying mechanism of neurodegeneration is an aberrantly activated form of development, triggered by levels of calcium influx inappropriate in the context of the more mature brain (Greenfield, 2013). Accordingly, the initial goal of this study was to see whether neuronal assemblies could be evoked in the basal forebrain, a key site of degeneration in Alzheimer's disease (Auld et al., 2002; Coyle et al., 1983), and if so,

Abbreviations: AChE, acetylcholinesterase; nAChR, nicotinic acetylcholine receptor; AI, prefrontal agranular insular cortex; AID, dorsal agranular insular cortex; AIV, ventral agranular insular cortex; aCSF, artificial cerebrospinal fluid; Aβ, amyloid Beta; BF, basal forebrain; Di-4-ANEPPS, 4-(2-[6-(Dibutylamino)-2-naphthalenyl] ethenyl)-1-(3-sulfopropyl)pyridinium inner salt; ELISA, enzyme-linked immunesorbent assay; fEPSP, excitatory post-synaptic potentials as recorded using field potentials; HDB, horizontal limb diagonal band; ISI, inter-stimulus interval; LO, lateral orbital frontal cortex; MS, medial septal nucleus; MWCO, molecular weight cut-off; NO, nitric oxide; PBS, phosphate buffer saline; ROI, region of interest; S1BF, primary somatosensory cortex; SEM, standard error of the mean; VDB, vertical limb diagonal band; VSDI, voltage-sensitive dye imaging.

* Corresponding author.
E-mail address: Scott.badin@neuro-bio.com (A.-S. Badin).

http://dx.doi.org/10.1016/j.neuropharm.2016.01.012
0028-3908/

whether any effects of the peptide might be age-dependent. We therefore investigated the possible modulatory effects of a synthetic version of AChE-peptide as a function of both brain-region and age using optical imaging with voltage-sensitive dyes, which enable a real-time visualisation of neuronal dynamics (Tominaga et al., 2000), and extracellular electrophysiology (field potentials).

Whilst the active sequence of AChE-peptide can be attributed to a specific 14 amino acid sequence originating from the C-terminus tail of AChE (T14) (Greenfield, 2013), exogenous AChE-peptide treatment in investigations from our lab has more recently involved a 30 amino acid peptide (T30) which includes the active T14 motif: the larger T30 is less likely to form fibrils when in solution, thereby possessing a higher stability and greater efficacy than T14 (Bond et al., 2009). Hence the T30 peptide was used throughout this study.

Given that the proposed mechanism of peptide-induced excitotoxicity would be of great relevance to furthering the development of effective drugs for halting the neurodegenerative process, we also tested whether a molecular variant would act as an antagonist, i.e. a cyclised variant of the active motif of AChE-peptide: 'NBP14' (Greenfield, 2015). The practice of cyclisation of compounds to improve their stability is not new (Goodwin et al., 2012) and has been exploited previously as a therapeutic strategy (Haworth et al., 1999; Hess et al., 2008). However, to the best of our knowledge, cyclisation of a peptide to act as a blocker of its endogenous, linear counterpart in relation to neurodegenerative disorders is unprecedented.

In rat brain slices, effects of exogenous peptide (T30) on assembly dynamics in basal forebrain were investigated and contrasted with those in the cortex and at different ages (p14 and p35-40), and compared with levels of endogenous AChE-peptide. Any effects of the peptide, which may contribute to the processes of neurodegeneration, were then tested for blockade by a cyclised variant of the AChE-peptide, NBP14.

2. Materials and methods

2.1. Preparation of rat brain homogenates for measuring AChE-peptide levels

The samples were prepared as follows: the brain sample was weighed before being placed in a dounce (tissue grinder) and 1 μL of PBS was added per 1 mg of brain material. The brain sample was homogenised by using the "loose" plunger. The "tight" plunger was used to further homogenise the material. The homogenised sample was collected in 2 mL Eppendorfs and centrifuged for 15 min at 13,000 g, 4 °C. Once the centrifugation was finished, the supernatant was collected into 0.5 mL 30 KDa MWCO filters. The samples were filtered by centrifuging through the filter for 30 min at 13,000 g, 4 °C and protease inhibitor cocktail (Roche complete PIC 04693116001) was added to the filtrate. This was used for the ELISA for T14 peptide. Unfiltered rat brain homogenate supernatant was used to determine the concentration of protein of the initial sample using the Pierce assay and subsequently ELISA determination using T14 antibody as described in (Garcia-Rates S., Morrill P., Pottiez G., Badin A-S., Tormo-Garcia C., Heffner C. and Greenfield SA. (I) Pharmacological profiling of a novel modulator of the α7 nicotinic receptor: blockade of a toxic peptide increased in Alzheimer brain.).

2.2. Preparation of brain slices and ex-vivo recordings

Coronal rat brain slices were prepared according to the procedure described in (Badin et al., 2013) but this time containing either agranular insular cortex, primary somatosensory cortex or basal forebrain (+0.70 and −0.26 millimetres (mm) from bregma (Paxinos and Watson, 1998)). Extracellular electrophysiology (field potentials) and optical imaging using voltage-sensitive dyes was then performed as previously described (Badin et al., 2013).

2.3. Preparation of exogenous peptides

Acetylcholinesterase (AChE) C-terminus 30 amino acid peptide (T30; sequence: 'N' – KAEFHRWSSYMVHWKNQFDHYSKQDRCSDL), the 15 amino acid inert part of the T30 (T15; sequence: 'N' – NQFDHYSKQDRCSDL) as well as the cyclic version of the active 14 amino acid region of T30 (NBP14; sequence: c[AEFHRWSSYMVHWK]; 'c[]' = cyclic, N-terminal to C-terminal lactam) were all prepared as described in (Garcia-Rates S., Morrill P., Pottiez G., Badin A-S., Tormo-Garcia C., Heffner C. and Greenfield SA. (I) Pharmacological profiling of a novel modulator of the α7 nicotinic receptor: blockade of a toxic peptide increased in Alzheimer brain.). When starting an experiment, aliquots were thawed and added to 'recording' aCSF as necessary, which was then perfused into the bath at a constant rate of 2.0 mL/min using a Minipulse 3 peristaltic pump (Gilson Scientific Ltd., Bedfordshire, UK). Perfusion conditions were 25 min in duration.

In the present investigation, the term 'AChE-peptide' refers to any peptide derived from the C-terminus of AChE and which has bioactivity at α7 nicotinic acetylecholine receptors, 2 different preparations of this peptide have previously been used: a 14 amino acid version (T14) (Badin et al., 2013) and a 30 amino acid version (T30, used here). Even though these two peptides act via the same mechanism of action, the T14 peptide has been found to come out of solution and create fibrils, hence why the T30 is preferred in the present investigation (Bond et al., 2009).

2.4. Data analysis and statistics

Experiments were carried out with simultaneous extracellular electrophysiology (field potentials, fEPSP) and VSDI monitoring of evoked population activity (See Fig. 1D i). Field potential records produced 53 data frames (800 ms in length each) per perfusion condition (25 min total – 10 min of acclimatisation followed by 15 min of recording; 28 s ISI). Electrical stimulations elicited a large artefact which lasted 2–3 ms immediately after stimulation, whilst the fEPSP population activity trace deflection peak occurred 5–6 ms after initial stimulation. Field potentials data from each experiment were excluded only if 1) the magnitude of recorded fEPSP signal was too small (maximum deflection peak <2 standard deviations from baseline level) equating to a low signal-to-noise ratio for that particular experiment, or if 2) the fEPSP deflection was not easily discernible from the stimulation artefact, making it unclear where the stimulation artefact finished and where the population activity fEPSP deflection started. For each individual experiment, of the 53 data frames recorded per perfusion epoch (raw data), every 4 frames were averaged together to give a total of 13 'mean' frames per condition, using MatLab (v8.2.0.701; The Mathworks Inc., USA). The maximum point, whether due to a positive or negative deflection, between 4 and 7 ms was measured for every 'mean' trace and plotted as a trend graph on axes of response amplitude (y-axis) vs mean frame number (x-axis), as shown in Fig. 7.

VSDI data were recorded in 4 × 4 mm 2-dimensional images, equivalent to 100 × 100 pixels – each pixel being 40 × 40 micrometres (μm), from which critical data were extracted. As opposed to electrophysiology, VSDI data was not gathered throughout the experimental run, but in fact was recorded in discrete periods of time 15 min long (recording epochs, see Fig. 7). The ISI between stimulations was the same as for electrophysiology (28 s) and therefore, every recording epoch consisted of 32 successive

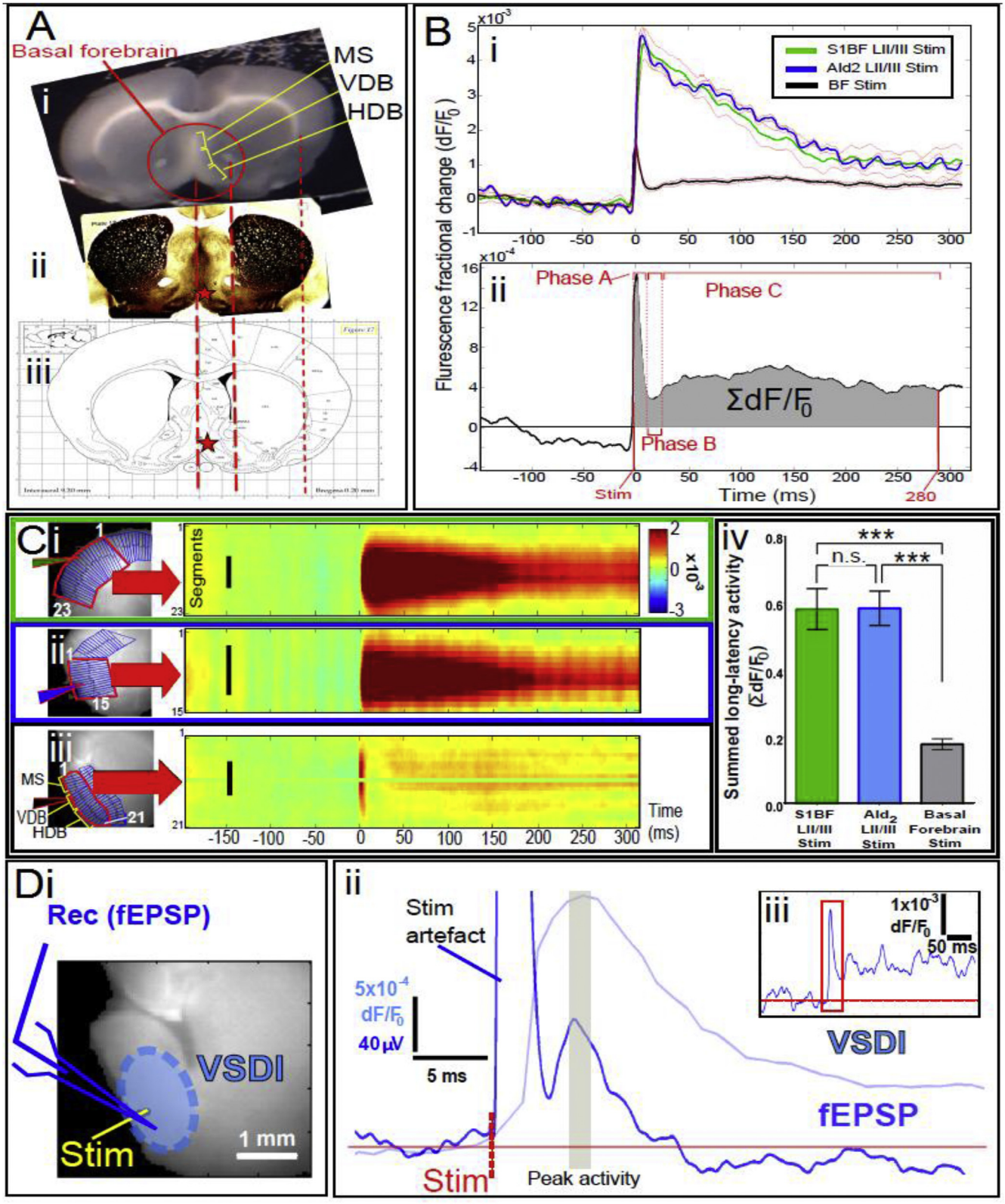

Fig. 1. Identification of Basal Forebrain (BF)-containing slices and characterisation of basal forebrain and cortical evoked population responses using voltage-sensitive dye imaging and electrophysiology: A. Sample photograph of a freshly-cut rat brain slice (i), containing medial-septal diagonal band complex, aligned with the corresponding plate (ii) and figure (iii), number 17, from the rat brain atlas(Paxinos and Watson, 1998). B i. Comparison of responses evoked by layer II/III stimulation in somatosensory barrel cortex (S1BF, n = 7), prefrontal association cortex (Ald_2, n = 7) and basal forebrain (BF, n = 30). ii. Close-up view of VSDI responses evoked in basal forebrain showing a distinct profile of response; the grey area under the curve represents the summed fluorescence fractional change data ($\Sigma dF/F_0$) measured for each recording epoch. C. VSDI analysis: selection and segmentation of region of interest (ROI), rasterization (Bourgeois et al., 2014) of ROI segments and plotting over time to produce 'space-time' maps of population activity for S1BF (i), Ald_2 (ii) and BF (iii); black scale bars are 1 mm in length. Colour bar units: dF/F_0. Summary bar graph (iv) of summed long-latency fluorescence fractional change for S1BF, Ald_2 and BF. D. Representation of simultaneous electrophysiology and VSDI recording setup (i) and resulting typical time-series from both techniques, best exemplified with sample traces

stimulations. The data from all 32 stimulations were then averaged into a single file for each experimental condition and analysed using a VSDI data analysis toolbox specially made for MatLab (Bourgeois et al., 2014). In short, this toolbox allowed for the selection of a fixed region of interest (ROI) geometry which could be applied to every slice, in order to extract and compound the data from an identical ROI across all slices and experimental conditions. For basal forebrain slices, the ROI was selected along the pial surface of the septal region to encompass the MS, VDB and HDB; for somatosensory cortex slices, the ROI was selected along the cortical mantle to encompass the entire barrel field; finally for association cortex slices the ROI was selected within the cortex and was focused on the lateral orbital cortex (LO), the dorsal and ventral agranular insular cortex (AID, AIV) (Paxinos and Watson, 1998), as electrical stimulations in the AID usually triggers 2-dimensional activity patterns which spread well beyond this cortical subarea's borders. Crucially, ROIs were selected to encompass the entirety of evoked VSDI responses. VSDI data, taken from the ROI, was then either plotted as a single averaged time series (Fig. 1B) or was plotted over space and time ('space-time' maps, Fig. 1C): such representations provided a good qualitative description of the data. In order to quantify VSDI data however, the area under the curve was calculated (summed fluorescence fractional change, Fig. 1B i) between the moment of stimulation (t = 0) and 280 ms after that; this method of quantification takes into account all the components of the immediate and longer-latency response. All statistical tests (one-way Analysis of Variance – ANOVA – unless stated otherwise) were performed using GraphPad Prism 6 (v6.05; GraphPad Software Inc., CA, USA), the data (both from ELISA and VSDI experiments) were all found to be normally distributed (data not shown). For all statistical tests, $P < 0.05$ was considered significant; data are expressed as mean ± S.E.M.

3. Results

3.1. Neuronal assemblies are site- and age-dependent

Coronal rat brain slices containing basal forebrain (BF) included the medial septal nucleus (MS), the nucleus of the vertical limb of the diagonal band (VDB) and the nucleus of the horizontal limb of the diagonal band (HDB), Fig. 1A. Within this region, electrical stimulation with a single 30 V pulse in slices from 14 day old animals triggered a distinct tri-phasic response (Fig. 1B) consisting of: a fast rise and decay component within the first 20 ms (ms) after stimulation (phase A), a short (15–20 ms) period of quiescence in activity (phase B), which ended when the basal forebrain showed a rebound, and a long-latency population activity lasting longer than 300 ms (phase C). This long-latency response features a slow rise and a slow decay, and for the purposes of this study, a cut-off boundary was set, encompassing the most active part of the long-latency rebound activity, at 280 ms after stimulation (Fig. 1B ii).

The activity seen in the basal forebrain in this third phase (C) was conspicuously different from that of two cortical areas reported here: the prefrontal association cortex (AId_2) and primary somatosensory cortex (S1BF). Basal forebrain responses were of significantly lower amplitude and more diffuse in nature (Fig. 1C i–iv) i.e. not clustered around the locus of stimulation. By contrast, assembly profiles in both sensory and association cortices in rats of the same age show a bi-phasic response of much greater amplitude, consisting of a very fast (10–15 ms) rise, immediately followed by a slow (200–300 ms) decay back towards baseline level (Fig. 1B ii), where fluorescence intensity peaks in the centre of the response, around the approximate locus of stimulation. Basal forebrain responses also show a much reduced signal, with VSDI responses on average ≈ 68% less extensive, $F(2, 41) = 99.41$, $p < 0.001$, with significant differences between S1BF and BF as well as AId_2 and BF (Fig. 1B i and C i-iv), than those evoked in both regions of neocortex tested, which were indistinguishable from each other (Fig. 1B i). Fig. 1D depicts the way in which VSDI and field potential data were simultaneously acquired in the present investigation (panel i). Resulting sample VSDI (light blue) and field potential (dark blue) recording traces from such a setup are superimposed in panel ii, illustrating the complementarity of both techniques used to monitor meso-scale neuronal dynamics in real-time: both VSDI and electrophysiology generate a peak in recorded population activity at exactly the same time, i.e. 5–6 ms after stimulus delivery.

As well as regional differences in population activity, age-dependent differences were also found across all three brain regions: Fig. 2 shows the effect of overall cerebral maturation on the extent of evoked population activity, recorded using VSDI, in cortex and basal forebrain. Highly significant age-related decreases were seen in both S1BF, $t(10) = 4.49$, $p < 0.001$, one-tailed un-paired t-test (Fig. 2A; 73.8 ± 5.6% decrease), and also AId_2, $t(11) = 8.31$, $p < 0.001$, one-tailed un-paired t-test (Fig. 2B; 79.4 ± 5.2% decrease). Similarly, significant difference in overall signal magnitudes were observed between evoked activity from p14 basal forebrain compared to that evoked in p35-40 rats, $t(33) = 2.71$, $p = 0.0052$, one-tailed un-paired t-test (Fig. 2C; 47.4 ± 3.7% decrease).

The VSDI signal recorded during stimulation was processed and displayed over space and time, with a resolution of micrometres (μm) and milliseconds (ms), respectively, in summary 'space-time' maps (Figs. 1C and 3A & B). Specifically, in the basal forebrain, phase A showed a much reduced peak activity in the older group (p35-40), as well as a much longer latency for phase B and a somewhat lower amplitude for phase C (Fig. 3A versus Fig. 3B) compared to younger animals. As a benchmark against previously published research from our lab on the effects of synthetic AChE-peptide in p35-40 rat association cortex (Badin et al., 2013), the effects of this agent were first assessed on basal forebrain population activity in rats of the same age (p35-40). As previously found in older animals, T30 perfusion was not found to induce any significant changes in evoked long-latency activity within p35-40 basal forebrain over time, $F(1.59, 6.36) = 0.86$, $p = 0.44$ (Fig. 3C), however VSDI data showed there to be a potent trend of decreased long-latency activity throughout the recording, with the greatest decrease seen during the 3rd T30 perfusion (75 min after the start of experiment, and 55 min after the start of the T30 perfusion).

3.2. Endogenous AChE-peptide brain content and assembly size decrease in parallel during development

Levels of endogenous AChE-peptide in whole rat brains were revealed by ELISA to be also age-dependent, showing a decreasing level between p7 and p14 rats (**p7**: 12.45 ± 0.51 μg/mg protein, n = 4; **p14**: 10.84 ± 0.42 μg/mg protein, n = 4; red line; Fig. 4A) and even greater reduction between p14 and p35-40 rats (**p35-40**: 8.51 ± 0.24 μg/mg protein, n = 4; red line), there was a significant

superimposed and phase-locked (ii). VSDI trace in light blue, electrophysiology trace in dark blue: this panel (ii) emphasises the complementarity of recorded VSDI and electrophysiology signal (simultaneously recorded from the same slice) showing both reach peak activity between 5 and 6 ms after stimulation (grey band).The inset (iii) shows the total VSDI trace (512 ms) from which the peak in ii was extracted (red rectangle). Significance levels: *** = P < 0.001; 'n.s.' = non-significant. Red bands in b. represent standard error of the mean (S.E.M.). (For interpretation of the references to colour in this figure legend, the reader is referred to the web version of this article.)

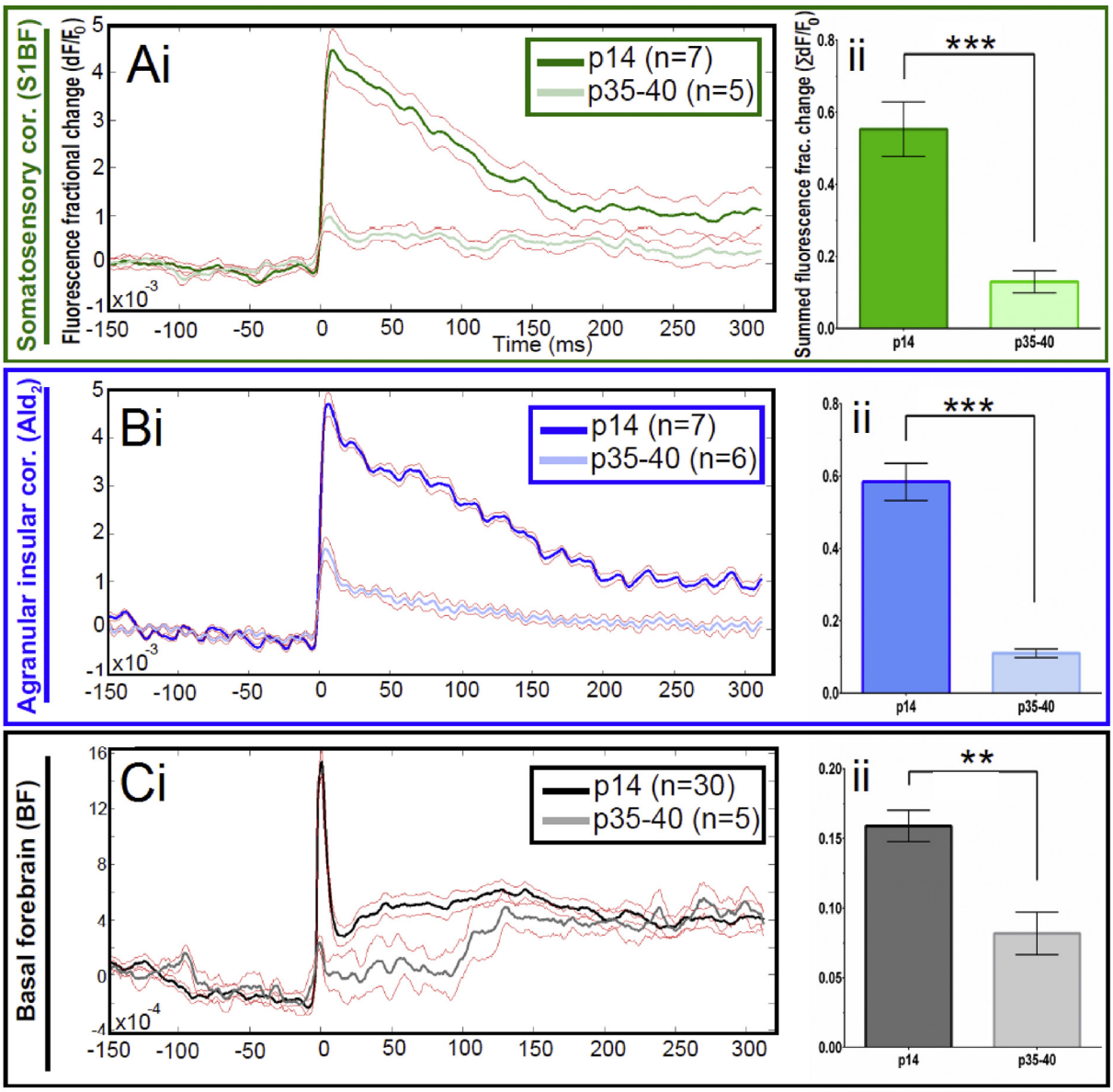

Fig. 2. Age-dependent decrease in VSDI signal from evoked responses in cortex and basal forebrain: Response time series from VSDI experiments (i) and resulting bar graphs of summed fluorescence fractional change normalised to their respective p14 maxima (ii) elicited from stimulation in layer II/III of p14 and p35-40 S1BF (A), AId_2 (B) and basal forebrain (C). Responses show a significant age-dependent decrease in recorded signal in all brain areas studied, with a larger decrease seen in cortex than in basal forebrain. Significance levels: * = P < 0.05; ** = P < 0.01; *** = P < 0.001; 'n.s.' = non-significant.

effect of age on endogenous AChE-peptide brain content between p7 and p14 rats as well as p14 and p35-40 rats, $F(5, 33) = 596.2$, $p < 0.001$. AChE-peptide levels stabilise in older animals, with no significant difference in content between p35-40 and p60 rats (**p60**: 8.18 ± 0.09 μg/mg protein, n = 12; Fig. 4A). Similarly, the extent of evoked population activity was measured using VSDI in p14 and p35-40 rats and compared to their respective age-dependent AChE-peptide content. The AChE-peptide content and the emitted fluorescence decrease by 21.6% and 47.4% respectively, between the two age groups: the summed fluorescence emitted within the ROI post-stimulus was found to be significantly different between p14 (0.156 ± 0.019 $\Sigma dF/F_0$; n = 30) and p35-40 rats (0.082 ± 0.014 $\Sigma dF/F_0$; n = 5; Fig. 4A, grey bars), as tested previously (Fig. 2C). In addition, differences in morphology could be seen directly with the naked eye between p14 and p35-40 brain slices (Fig. 4B). More specifically, there appears to be a noticeable increase in white matter within older rat brain slices compared to younger brain slices (Fig. 4B, red ellipse, orange arrow, yellow area), especially obvious in the appearance of the anterior commissure (Fig. 4B, red arrows).

3.3. T30 peptide modulates assembly activity and is blocked by a cyclised variant

A series of control experiments was performed to ensure that any apparent effect of the peptide was not attributable merely to the long time-course of recording, nor to any non-specific drug effects. All three recording epochs (epochs 1–3) showed no significant differences over hour-long recording windows (Fig. 5A iii; n = 9), $F(2, 24) = 0.47$, $p = 0.63$. Moreover, the inert part of the T30 peptide (T15, 2 μM) (Bond et al., 2009), although affecting the spatial profile, did not produce any changes in recorded summed

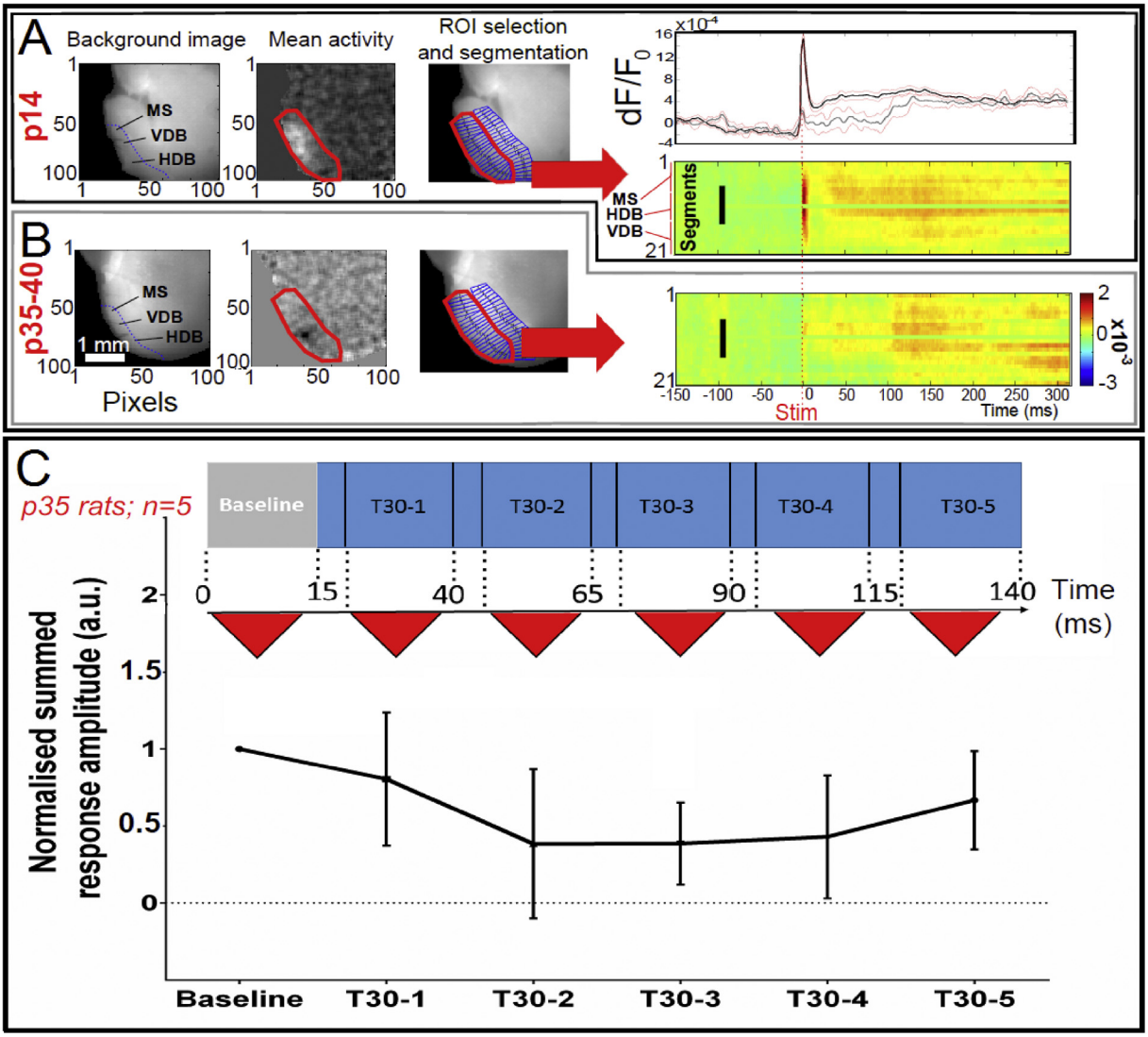

Fig. 3. Basal forebrain age-dependent assembly dynamics and effects of T30 peptide: Panels showing the raw data image background, the mean activity averaged between 0 and 10 ms after stimulation, the selection and segmentation of the ROI for VSDI data analysis and subsequent plotting of recorded data on space-time maps for p14 (A, n = 30) and p35-40 rats (B, n = 5). Black scale bars are 1 mm in length. The time series from p14 and p35 rats, in panel A, has its time axis phase-locked with that of the space-time maps in panels A and B for appropriate temporal comparison of spatial activity patterns with time series traces. Colour bar units: dF/F_0. C. Experiments investigating the longer-term effects of T30 on p35-40 rats basal forebrain population dynamics (140 min total in duration). (For interpretation of the references to colour in this figure legend, the reader is referred to the web version of this article.)

fluorescence, maintaining the same overall level of activity (Fig. 5B iii; n = 5), $F(2, 12) = 0.0079$, $p = 0.99$.

Administration of T30 (2 μM) caused a significant decrease in overall post-stimulus activity, $F(1.72, 34.29) = 7.59$, $p = 0.0028$, (Fig. 6A iii, middle bar; 42.7 ± 11.1% decrease normalised to respective baseline activity; n = 21) compared to baseline, and a decrease of the same general magnitude was seen when compared to the Control 2 period of recording (Fig. 5A iii; 56.7 ± 10.6% decrease normalised to respective baseline; n = 9), $t(28) = 3.11$, $p = 0.0021$, one-tailed un-paired t-test. This potent inhibition on overall population response is characterised by a much longer inhibitory phase B and a lowered amplitude in phase C. Finally, the candidate blocker of AChE-peptide, when applied alone, did not induce any significant changes in basal forebrain population dynamics, $t(4) = 0.22$, $p = 0.83$, two-tailed paired t-test (Fig. 6B; n = 5). However, when T30 was perfused in the presence of NBP14, the inhibition induced by T30 was reversed (Fig. 6A iii, purple bar; 92.5 ± 7.5% of baseline level; n = 21), $F(1.72, 34.29) = 7.59$, $p = 0.0028$. Fig. 6C summarises the normalised data from the four different experiments (no drug controls, T15, T30 & NBP14 and NBP14 experiments) carried out in p14 rats basal forebrain: taken together, these experiments show that basal forebrain recordings remain stable for at least 65 min under the current experimental paradigm, and that the addition of a small non-specific peptide (T15) to the perfusion aCSF does not alter population dynamics in any significant way. Furthermore, perfusion of AChE-peptide containing the bioactive peptide motif (T30) induces a significant reduction in the extent of long-latency population activity, which is reversed by addition of NBP14.

In five experiments monitoring fEPSP, where the signal was clearly discernible above noise, low amplitude upward deflections were consistently observed (Figs. 1D ii and Fig. 7), irrespective of whether the recording electrode was placed in the VDB (ventral to the locus of stimulation, as shown in Fig. 1D ii, n = 3 of 5) or the MS (dorsal to the locus of stimulation, n = 2 of 5). In contrast to data obtained in p14 rats using VSDI, perfusion with neither T30 nor

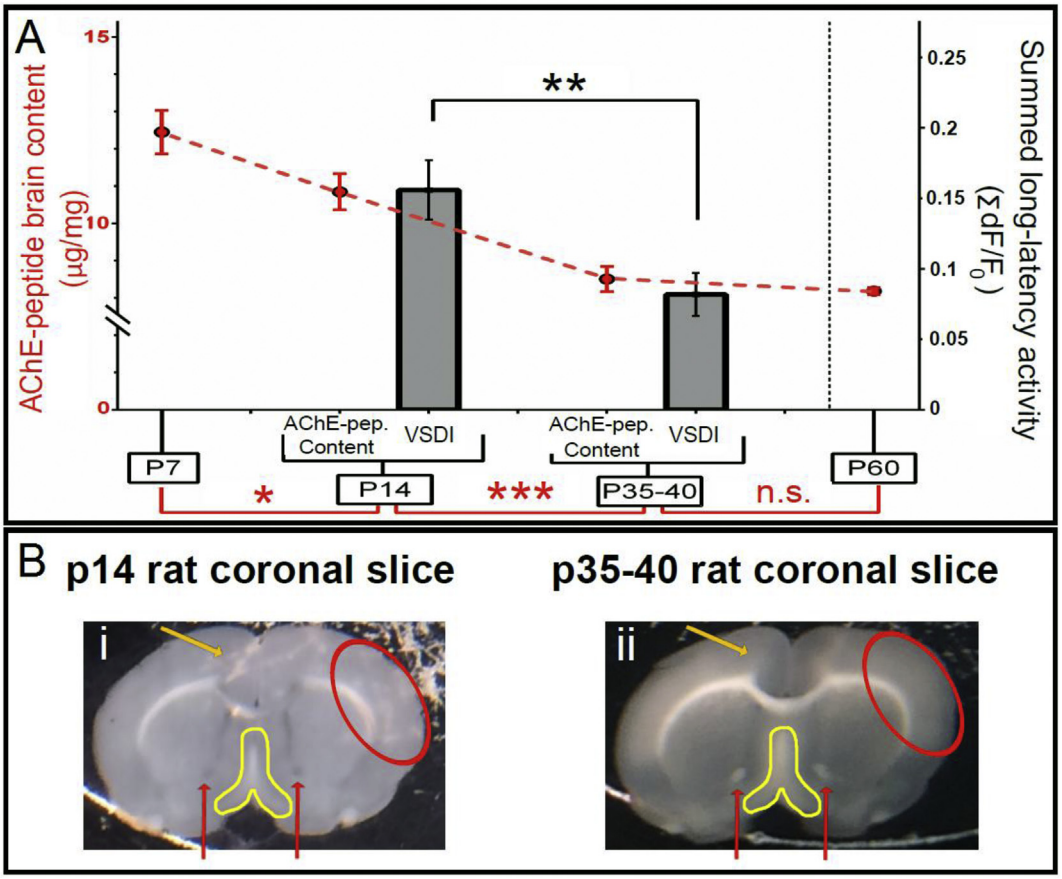

Fig. 4. Correlated age-dependent decrease in basal forebrain population activity and AChE-peptide brain content: A. Bar graph featuring age-specific AChE-peptide (T30) content assayed using ELISA in whole brain homogenate from p7, p14, p35-40 and p60 rats (red line, left y-axis), showing an age-dependent decrease, with a significant drop between p14 and p35-40 rats, and a stabilisation of brain peptide content with maturation. In this graphical representation, ELISA assays were done on p7, p14 and p35-40 rats within the same experiments, while those of p60 rats constituted a separate study. Likewise, the magnitude of assembly activity was found to decrease significantly between p14 and p35-40 rats (grey bars, right y-axis). B. Pictures (×10 magnification) taken of freshly-cut slices containing basal forebrain diagonal band complex (MS, VDB & HDB, yellow area) from p14 (i) and p35-40 (ii) rat brains. Noticeable changes can be seen in slice morphology between the two age groups: slices in younger animals seemed less opaque than in older rats – the background of the well can be seen through the slice in p14 as opposed to p35-40 slices (specifically: as shown by the orange arrow and red ellipse). Additionally, there appears to be a marked increase in white matter content in slices from older animals, especially in the basal forebrain (yellow area) and cortex, where layer IV is distinguishable in p35-40s but not in p14 rats (red ellipse), as well as in the anterior commissure (red arrows). Significance levels: * = $P < 0.05$; ** = $P < 0.01$; *** = $P < 0.001$; 'n.s' = non-significant. (For interpretation of the references to colour in this figure legend, the reader is referred to the web version of this article.)

NBP14 significantly altered the profile of fEPSP signals throughout the entire recording window (Fig. 7A). A similar lack of effect was also observed in p35-40 rat basal forebrain, n = 4 (Fig. 7B) even after 2 h of perfusion.

Although T30 induced a net inhibition (n = 21; Fig. 8A i) in recorded VSDI signal of ≈43% in the basal forebrain of p14 rats, this value actually includes a minority of instances where negligible or marginally positive effects were seen during T30 perfusion (Fig. 8A ii). However in all cases, regardless of the polarity of the effect induced by T30, population activity was invariably reversed back towards its respective baseline level when NBP14 was co-perfused: this phenomenon is highlighted more clearly, using actual data points taken from the n = 21 raw data pool, for both T30-induced decreases and increases (Fig. 8A i & ii, respectively). Plotting the magnitude of summed fluorescence fractional change for baseline condition (Fig. 8A iii; x-axis; $\Sigma dF/F_0$) against the change in summed fluorescence fractional change between baseline and T30 perfusions (y-axis; $\Delta\Sigma dF/F_0$) yields scatter graphs of the raw data from which a correlation can be derived: the greater the initial baseline response, the greater the change in summed fluorescence as a result of T30 perfusion, this correlation was found to be highly significant $r(19) = 0.58$, $p < 0.001$. Similarly, Fig. 8B shows that the greater the change from baseline due to T30 perfusion, the greater the reversal once NBP14 was added to the perfusate: this correlation was also found to be highly significant $r(19) = 0.51$, $p < 0.001$.

4. Discussion

4.1. Neuronal assemblies as a sensitive index of meso-scale brain processing

Assemblies operate at a level of brain organisation that provides a valuable functional link between 'bottom up' cellular mechanisms and 'top down' cognitive ones. Optical imaging of this relatively unfamiliar phenomenon using voltage-sensitive dyes has now been established as a powerful means for studying neuronal dynamics with an unprecedented spatial resolution in real-time (Berger et al., 2007; Kuhn et al., 2008; Yuste et al., 1997). When compared with conventional electrophysiological recording of field potentials, both signals show correlated activity peaks, thereby confirming that VSDI signals are not artefactual, and reflect relevant physiological processes. The VSDI peak duration is much broader than that of field potentials however, possibly as a result of the difference in the size of the receptive field of the two techniques: VSDI compiles data

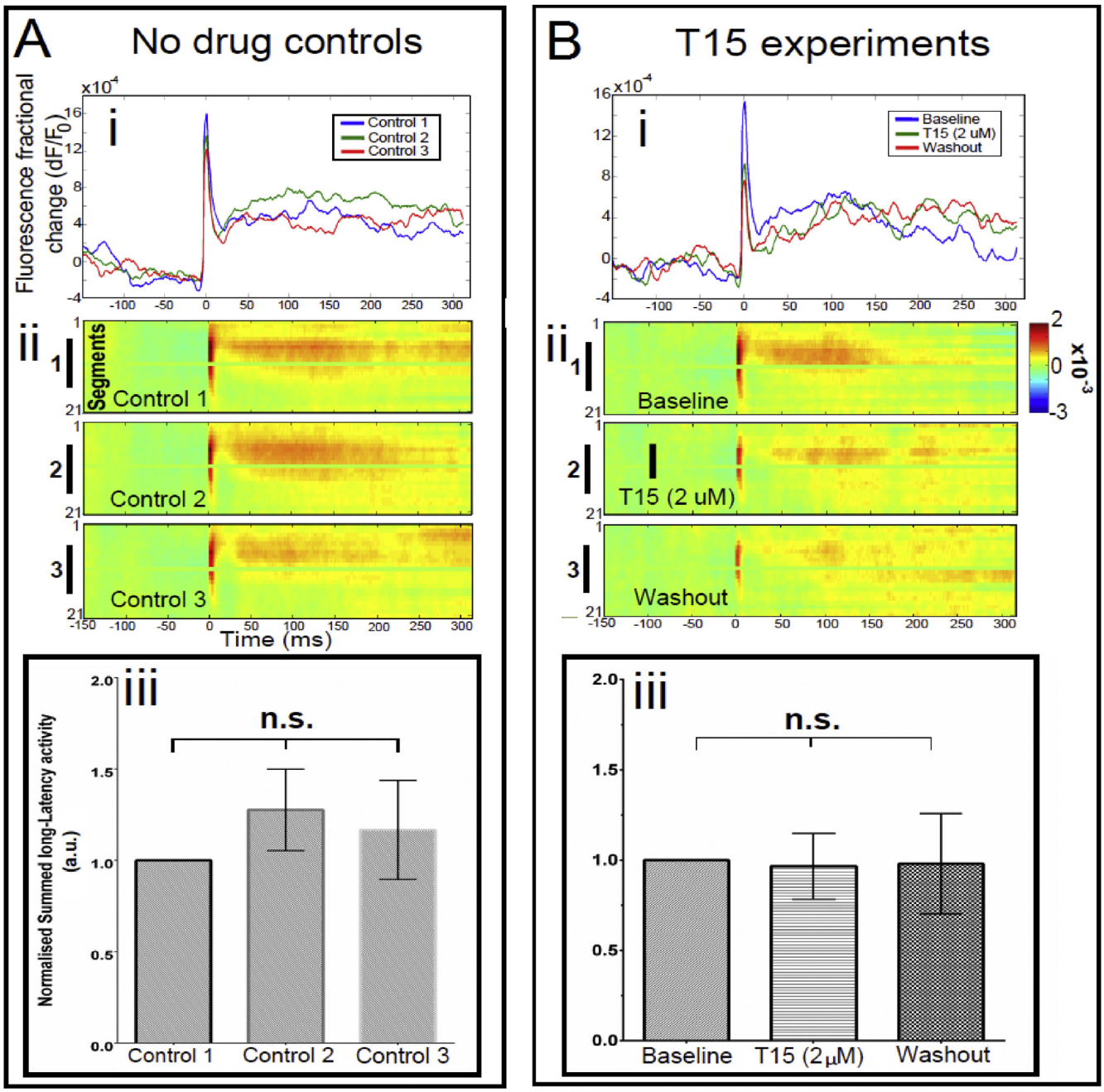

Fig. 5. Control experiments in p14 rat basal forebrain: A. Control experiment (n = 9) carried out over a 65 min time-window (15 min-long recording epochs interspersed with 10 min-long no recording epochs): 'Control 1–3' – only small, non-significant changes in long-latency assembly dynamics were seen, confirming the health of the preparation and stability of the recording. Panel A shows the averaged time series (i), the equivalent averaged space-time maps for each recording epoch (ii) and the summary histogram of summed fluorescence (iii) B. Results from an identical experimental paradigm run using 2 μM T15 (n = 5) are presented in the same fashion: VSDI time series (i) corresponding space-time maps (ii) and resulting bar graph of summed fluorescence (iii). Despite an apparent change in response profile seen on space-time maps of T15 control experiments (B ii), no significant change is seen in the resulting magnitude of summed fluorescence (B iii): as can be seen in the time series graphs (B i), this is because the area under the curve of the baseline condition is approximately equal to that of the T15 and washout conditions, albeit with an altered profile of response. The black scale bar is 1 mm in length and applies to all 6 space-time maps. Colour bar units: dF/F_0. Significance levels: 'n.s.' = non-significant. (For interpretation of the references to colour in this figure legend, the reader is referred to the web version of this article.)

from a two-dimensional region of interest (ROI), while field potentials report changes in electrical gradient from a single discrete point within that region. Electrical pulses delivered to the MS, within the ROI focused on the diagonal band complex (see Materials & Methods), triggered a large stimulation spike (0–15 ms after stimulation) in population dynamics followed by more latent diffuse network activity (15–280 ms after stimulation). Since some of the fluorescence recorded during this initial stimulation spike may result from unspecific neuronal depolarisation, to some extent bypassing receptor-mediated activity, both the stimulation spike as well as the long-latency activity were calculated in a single measure as the sum of fluorescence recorded from the moment of stimulation until the end of the recording window.

Previous investigations with VSDI have concentrated on activity

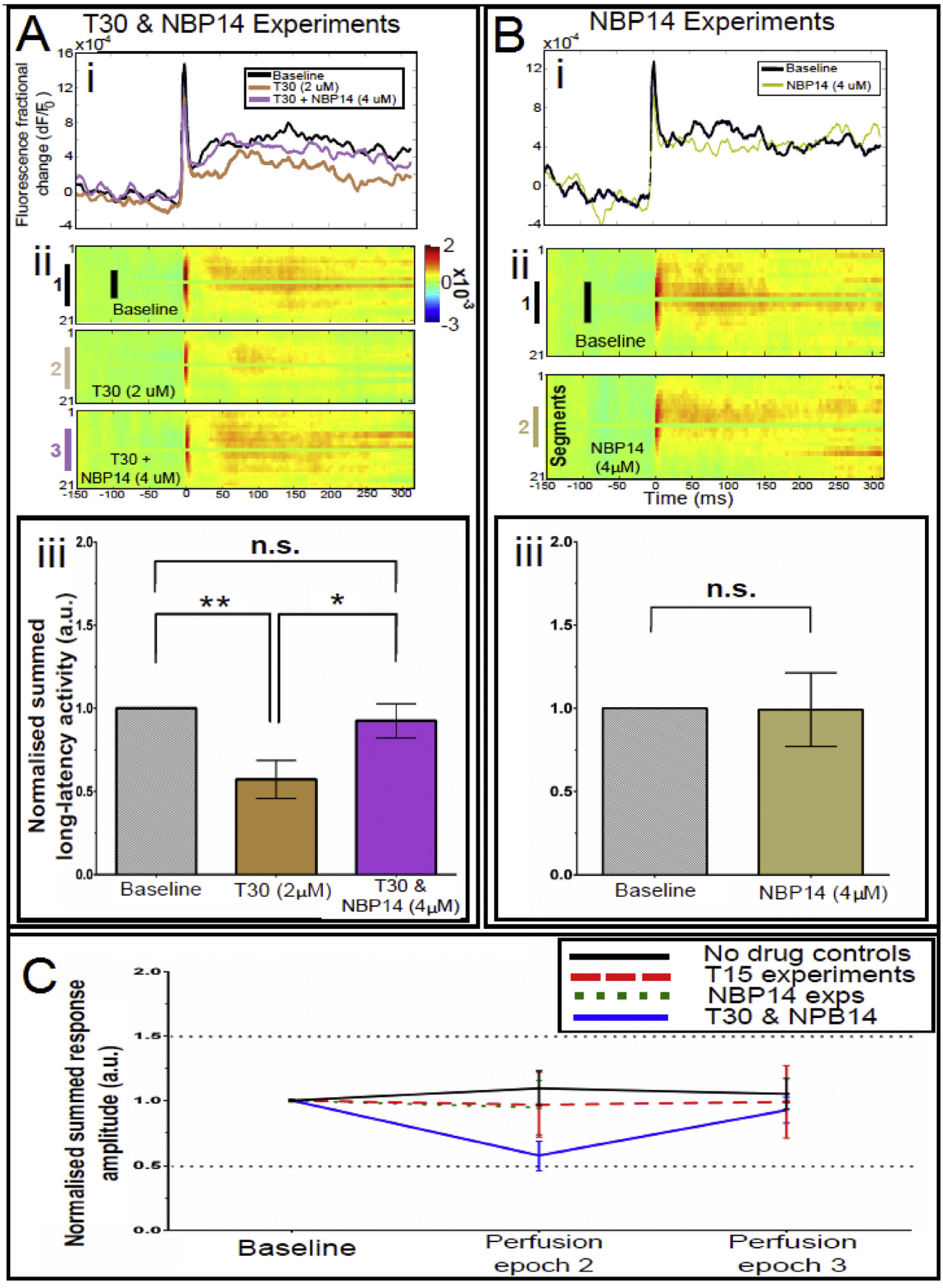
A
T30 & NBP14 Experiments
Fluorescence fractional change (dF/F0)
Baseline
T30 (2 uM)
T30 + NBP14 (4 uM)
Baseline
T30 (2 uM)
T30 + NBP14 (4 uM)
Normalised summed long-latency activity (a.u.)
n.s.
**
*
Baseline
T30 (2μM)
T30 & NBP14 (4μM)
B
NBP14 Experiments
Baseline
NBP14 (4 uM)
Segments
NBP14 (4μM)
Time (ms)
n.s.
Baseline
NBP14 (4μM)
C
No drug controls
T15 experiments
NBP14 exps
T30 & NPB14
Normalised summed response amplitude (a.u.)
Baseline
Perfusion epoch 2
Perfusion epoch 3

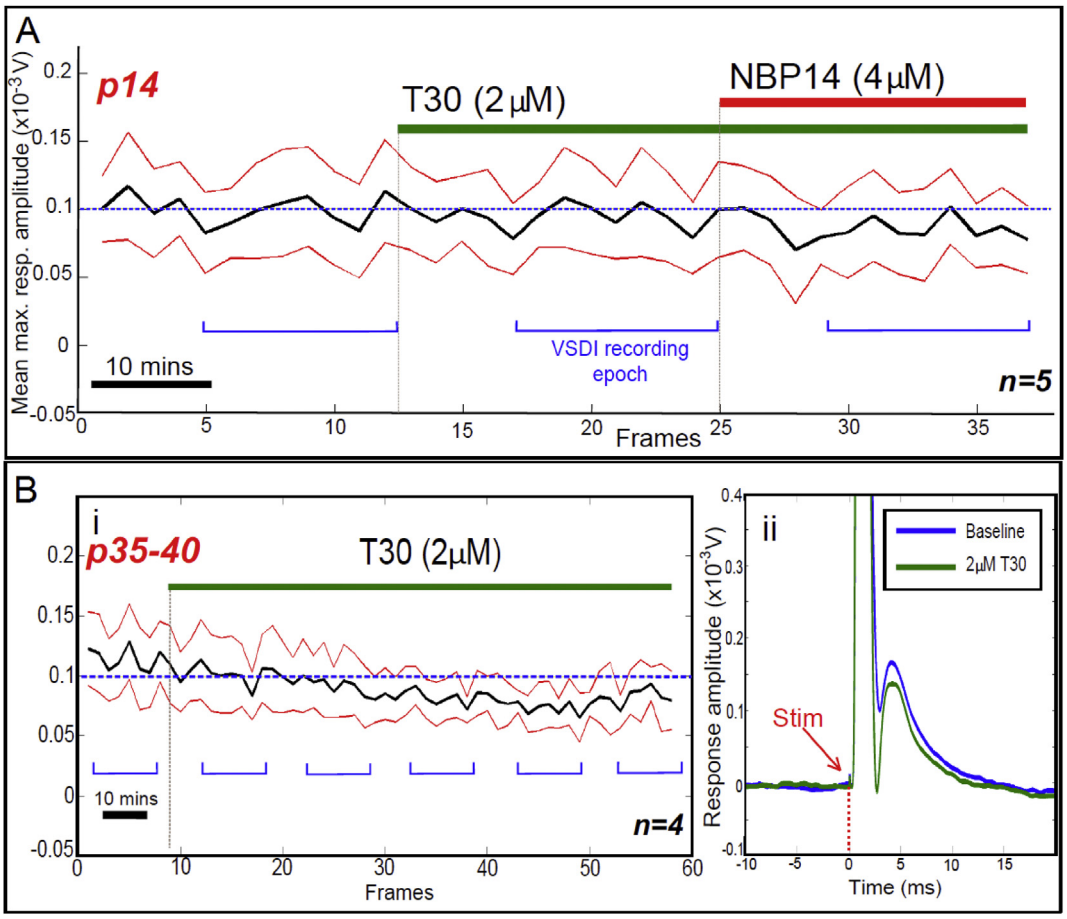

Fig. 7. Field potential recordings in p14 and p35-40 rat basal forebrain during T30 perfusion. A. Summary trend graph of maximum amplitude of evoked trace deflection in p14 rats, showing no significant changes induced by either T30 or co-perfusion with NBP14 (n = 5). Red traces indicate ± standard error of the mean (S.E.M). A sample trace of field potential deflection recorded in p14 rat basal forebrain is shown in Fig. 1D ii. B. Summary trend graph of maximum amplitude of evoked trace deflection in p35-40 rats (i; n = 4), showing no change. Panel ii shows a sample field potential deflection trace from p35-40 rat basal forebrain. The baseline trace (blue) represents all traces recorded during baseline, while the T30 trace (green) represent all the traces recorded during the last 'VSDI recording epoch' (for p35-40, **Bi**). (For interpretation of the references to colour in this figure legend, the reader is referred to the web version of this article.)

either *in vitro* or *in vivo*, in the cortex. In this study, two cortical areas were selected for reference, one where assemblies have already been characterised (i.e. Prefrontal association cortex, AId_2) (Badin et al., 2013), and for comparison a well-studied area of sensory cortex (primary somatosensory cortex, S1BF) (Berger et al., 2007). Aside from accessibility, *in vitro* but most importantly *in vivo*, experiments on the cortex have proved popular because cortically-evoked activity is much more extensive, with slower dynamics, than normally seen in sub-cortical structures (Golomb et al., 1996): one exception is the hippocampus, classified as '*allocortex*' which, like neocortex, is laminated in structure with discrete processing and integration abilities, thus conferring neocortical-like population dynamics (Mann and Greenfield, 2003; Tominaga et al., 2000). However since the aim here was to use VSDI to explore a basic neuronal mechanism that could underlie a link between development and Alzheimer's disease (Greenfield, 2013), the basal forebrain was the focus of investigation, as it is a primary site of cell loss in the disease (Auld et al., 2002; Coyle et al., 1983): this area has the same embryological provenance and shares common properties with brainstem neurons participating in a range of neurodegenerative disorders (Greenfield and Vaux, 2002; Woolf, 1996). To the best of our knowledge, this is the first report of optical imaging in the basal forebrain, and the first description of the distinct profile of neuronal assemblies generated in this sub-area.

4.2. Regional differences in assembly dynamics

Assemblies generated in basal forebrain featured much lower amplitudes and much faster paced dynamics, reminiscent of 'lurching' waves (Golomb et al., 1996), as previously described in other sub-cortical structures such as the thalamus, albeit using electrophysiology. In any event, the profiles of evoked responses in basal forebrain were conspicuously different from those recorded in the two regions of cortex, indicating different population

Fig. 6. Effect of T30 on meso-scale basal forebrain population dynamics and blockade with NBP14: A. Inhibition by T30 (2 μM, n = 21) of p14 basal forebrain long-latency population activity and reversal of effects when co-perfused with the candidate blocker NBP14 (4 μM), displayed as averaged time series (i), space-time maps (ii) and resulting bar graph of normalised overall summed fluorescence (iii) across all three treatments. B. Control experiment with NBP14 (4 μM, n = 5) data, showing no effect on population activity, displayed in the same organisation as A. Scale bars on space-time maps are 1 mm in length. C. Summary line plot comparing the normalised VSDI data from the four experiments shown in Figs. 5 and 6. Colour bar units: dF/F_0. Significance levels: * = $P < 0.05$; ** = $P < 0.01$; 'n.s' = non-significant. (For interpretation of the references to colour in this figure legend, the reader is referred to the web version of this article.)

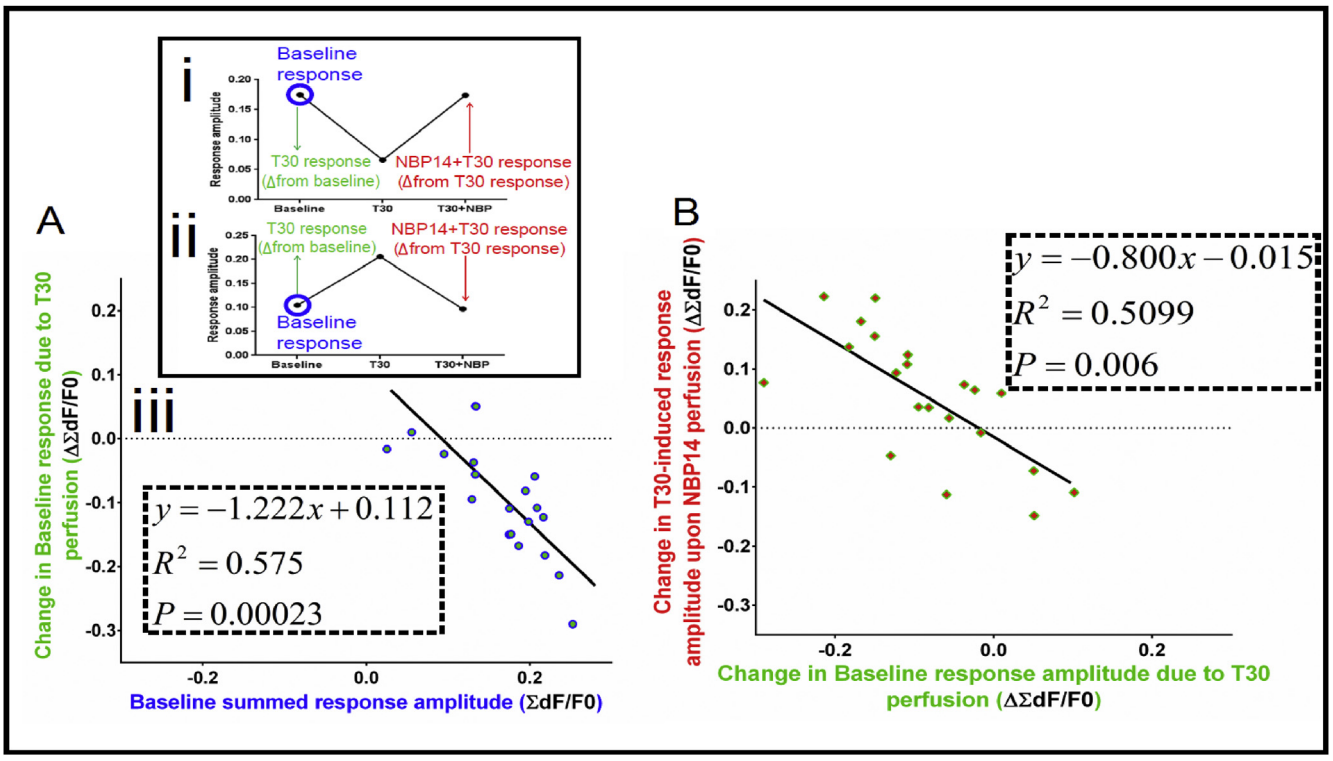

Fig. 8. Correlation of basal forebrain population activity with magnitudes of drug-induced effects: A. Individual data points from T30 & NBP14 VSDI experiments, highlighting the change in response magnitudes between perfusion epochs, in most cases showed inhibition induced by T30 perfusion (17 out of 21 experiments), however a few cases of increased or unchanged activation were seen (4 out of 21 experiments). Sample data points were selected to show the net effect of T30-induced inhibition (i) and excitation (ii). The summed fluorescence of baseline responses, for all 21 experiments, were plotted against the magnitude of change induced by T30 (iii). This data representation shows a clear correlation ($P < 0.001$) where low baseline responses yielded very little change, or excitation, when perfused with T30, whilst high baseline responses yielded greater inhibition upon T30 application. B. Similarly, the magnitude of change in summed fluorescence as a result of T30 perfusion was plotted against the change then induced by T30 and NBP14 co-perfusion. Here the correlation ($P < 0.01$) highlights the way in which the more T30 induced inhibition, the more NBP14 restored activity, whilst the more T30 induced an increase in summed fluorescence the more inhibitory the effects of NBP14: in either case NBP14 annulled the modulatory effects of T30.

dynamics in basal forebrain, possibly reflecting major differences in cytoarchitecture between subcortical and cortical brain regions: the medial septal/diagonal band complex (MS, VDB, HDB) consists of a highly heterogeneous mix of cholinergic, GABAergic, glutamatergic and nitric oxide (NO) synthase-positive cells (Sotty et al., 2003; Wang et al., 2006) which, together, form a hub of cells from which multiple cholinergic projections originate and extend primarily to the hippocampus and the cortex (Senut et al., 1989).

A functional role for the basal forebrain would therefore be to target higher brain regions in a diffuse manner differing greatly from processes within neocortex, organised to amplify afferent information by prolonging its activity, thus increasing the time-window for information processing (Singer, 1993). The crucial issue however is that the basal forebrain can generate assemblies, suggesting a process of local, large-scale neuronal cohesion that will have functional implications, particularly in development.

4.3. Age-dependent differences in AChE-peptide abundance and recorded VSDI signal

In this study, animals were selected at four developmental stages: p7 – infants, p14 – juveniles, p35-40 – young adolescents and p60 – young adults (Andreollo et al., 2012). The greatest difference in AChE-peptide brain content was found between p14 and p35-40 rats – we therefore focused VSDI experiments on these two age groups, where there was a marked discrepancy: ≈70–80% reduction in VSDI signal in cortex and ≈47% reduction in signal from basal forebrain of older rats.

Since we observed an increase in opacity of slice tissue between the two age groups (p14 and p35), probably due to an increase in myelination (Nunez et al., 2000), the possibility arises that the decreases seen with assembly size were simply a result of reduced optical signal due to the decrease in exposed membrane space. However diverse other factors over-ride this potential artefact: firstly many other developmental processes take place in the maturation of rat brain between p14 and p35-40 which together could lead to a net reduction in recorded VSDI signal, in particular a reduction in the endogenous trophic agent AChE-peptide, as shown here. Secondly, the declining assembly size with age can be most readily explained by the fact that neuronal assemblies have already been shown to be particularly vigorous in neuronal plasticity (Devonshire et al., 2010). Thirdly, the acute changes apparent following application of T30 peptide in the cortex as well as basal forebrain of p14 rats, and by contrast to the lack of significant effects seen in older animals (as shown here and reported previously for p35-40 rats (Badin et al., 2013)), strongly suggests the effects are dependent on animal age, and almost certainly the result of a true physiological mechanism. Fourthly, the VSDI signal, in particular that is generated by Di-4-ANEPPS, reflects activity originating from neuronal cell bodies, axons and dendritic neuropil, but with the most significant input from the latter (Denk et al., 1990), which remains unmyelinated. Since the basal forebrain is part of a region known as the isodendritic core (Rossor, 1981), characterised by a conspicuous dendritic arbor, the contribution to the signal from these non-myelinated parts of the neuron would be substantial. This proposition is corroborated by the relative insensitivity of

electrophysiological recordings, which would have preferentially reflected axonal conduction and somatic activity. Comparison of field potential deflections presented here (Fig. 1D ii vs Fig. 7B ii) shows that with identical stimulation protocols similar response amplitudes were elicited in both p14s and p35-40 rats. In any event, these results provide justification for focussing the rest of our experiments on younger (p14) rats, as neuronal networks display a greater sensitivity to modulation by the peptide, as well as where VSDI produces greater activity patterns, with an increased signal-to-noise ratio compared those evoked in older animals.

Within the basal forebrain, these age-dependent differences in assembly dynamics are correlated with the respective levels of endogenous AChE-peptide, as suggested previously by the developmental dominance of a single catalytic sub-unit ('G1' AChE), from which the free peptide would have been cleaved, and which is recapitulated in Alzheimer's disease (Arendt et al., 1992; Saez-Valero et al., 1999). In the present study, the AChE-peptide content was assayed directly in whole brain homogenate using a highly selective custom-made antibody (Garcia-Rates S., Morrill P., Pottiez G., Badin A-S., Tormo-Garcia C., Heffner C. and Greenfield SA. (I) Pharmacological profiling of a novel modulator of the α7 nicotinic receptor: blockade of a toxic peptide increased in Alzheimer brain.) and measured across all age groups, each representing distinct stages in development. Though p7 rats were included in the ELISA evaluation, VSDI experiments could not be performed since it was not feasible to locate accurately basal forebrain at this early age. Similarly, VSDI experiments were not carried out in p60 rats, which showed a similar level of endogenous peptide as in younger p35 animals, and thus would give no further insight into the differential being studied in the two critical age points. However AChE-peptide brain content decreased throughout development, as seen in Fig. 4, in accordance with the proposition that the non-enzymatic functions of acetylcholinesterase arise from the actions of a peptide cleaved from its C-terminus, and that the production of this signalling peptide is linked to neuro-development (Greenfield, 2013). Previous research had already implicated AChE-peptide, which possesses a conserved amino acid sequence with β-amyloid (Aβ) (Greenfield and Vaux, 2002), as a pivotal molecule in Alzheimer's disease. More specifically, both AChE-peptide and Aβ up-regulate calcium influx into neurons(Greenfield et al., 2004; Wu et al., 1995) in turn leading to enhancement of neuronal outgrowth(Day and Greenfield, 2002; Soreq and Seidman, 2001; Webb and Greenfield, 1992), affecting neuronal plasticity (Day and Greenfield, 2002; Greenfield et al., 2004; Webb and Greenfield, 1992) and ultimately triggering apoptosis (Garcia-Rates et al., 2013; Loo et al., 1993). Taken together, these observations indicate a key developmental role of AChE-peptides and Aβ, mediated via potentiation of calcium currents into neurons, and explain how excessive or inappropriate activation would convert trophic actions into excitotoxicity (Eimerl and Schramm, 1994).

4.4. Effects of AChE-peptide and its blocker on assembly dynamics

Experiments performed over 65-min periods without any drug intervention ensured that any effects of T30 application were not attributable to changes in the overall condition of the slice over time. The same lack of effect also held for perfusion with an inert peptide sequence derived from AChE (T15), thereby eliminating the possibility of non-specific effects of peptide application. In contrast, perfusion of T30 induced decreases in evoked response magnitude over time, with inhibitions of 47% seen in p14 and 54% for p35-40 rats, yet only significantly different for younger animals, in accordance with previously published observations of T30 effects on prefrontal cortical meso-scale dynamics of more mature (p35-40) rats (Badin et al., 2013). In this earlier study, the actions of AChE-peptide were mediated via α_7-nAChRs, as has been shown also for inward currents in oocytes (Greenfield et al., 2004), neurite outgrowth and cell death in hippocampal organotypic cultures (Day and Greenfield, 2003), receptor expression in primary cell cultures (Bond et al., 2009) and long term potentiation in brain slices (Greenfield et al., 2004); most significantly the occurrence of these concurrent diverse trophic-toxic changes in neuronal cytoarchitecture have previously been documented in the basal forebrain of patients with Alzheimer's disease (Arendt et al., 1995). However the most conspicuous difference seen between young and old rats was the time taken to achieve maximum T30-induced inhibition, with full effect taking twice as long in the older group, suggesting a lower sensitivity of more mature neuronal networks to the effects of AChE-peptide; presumably as a result of physiological changes having taken place in older rat brains, which may include the declining level of AChE-peptide given its function as a trophic agent (Day and Greenfield, 2003). In young rat basal forebrain, T30-induced inhibition was significantly reversed by NBP14 ($P < 0.05$), the synthetic, cyclised version of the T14 peptide which was inert when applied alone. Importantly, the Companion paper (Garcia-Rates S., Morrill P., Pottiez G., Badin A-S., Tormo-Garcia C., Heffner C. and Greenfield SA. (I) Pharmacological profiling of a novel modulator of the α7 nicotinic receptor: blockade of a toxic peptide increased in Alzheimer brain.) provides complementary evidence of the detrimental cellular actions of both Aβ and AChE-peptide measured over protracted time-courses, including confirmation of the protective actions of NBP14 in PC-12 cells, a cell line described as a 'window on the brain' (Bornstein et al., 2012).

When experiments were repeated, testing the bioactivity of T30 and NBP14 by standard electrophysiological recordings, no effect was observed. However, if the inhibitory effects of the peptide observed previously had been simply due to suppression of somatic action potentials, then a depressant effect should have been observed here. VSDI using Di-4-ANEPPS reports changes in membrane potential across neuronal cell membranes, while the recorded signal is dominated by sub-threshold post-synaptic potentials (Berger et al., 2007): this optical imaging technique therefore provides a much more sensitive read-out of two-dimensional excitatory signal flow through neuronal tissue, including both supra-as well as sub-threshold dynamic changes in membrane potentials. The discrepancy between results from electrophysiology and VSDI shown here, most probably arises from the fact that significant population depolarisation must occur for electrophysiology to detect changes in electrical gradient within slices (supra-threshold events): in contrast VSDI reports the smallest of changes in membrane potential (all changes including sub-threshold events). The fact that no changes in response amplitudes were seen with electrophysiology suggests T30 induces the vast majority of its effects on sub-threshold neuronal dynamics, not detected by electrophysiology. Moreover, VSDI reflects changes in population activity over time *and* space, whilst extracellular electrophysiology merely identifies potential differences from a single discrete location over time; this discrepancy in receptive field of either technique may further explain the discrepancy reported here.

Consequently, the more sensitive method of VSDI revealed that the effects of T30 were not wholly inhibitory, but that magnitude and polarity of T30-induced changes were correlated ($P < 0.001$) with the extent of the pre-existing baseline response. When the exogenous molecule is then applied, it will further activate calcium channels where, in slices with low baseline responses associated with low levels of endogenous AChE-peptide, it will trigger enhanced excitatory responses as seen in a minority of cases (3–4 out of 21). In the majority of cases in the younger animals, where levels of AChE-peptide have been shown to be already high, the additive effect of exogenous peptide will inhibit calcium influx (Bon

and Greenfield, 2003; Greenfield et al., 2004) due to phosphorylation of the channels (Plant and Standen, 1981) accounting for the apparently depressant effect observed. VSDI signal between the two age groups is correlated with levels of endogenous peptide: hence it could be the case that in the four individual experiments with a low baseline, the optical signal is indicative of lower levels of endogenous peptide; with the opposite being true for experiments showing inhibition.

In conclusion, this study demonstrates for the first time that a modification in the activity profile of neuronal assemblies may serve as a physiological index of developmental status that is parallelled by a change in cerebral levels of an endogenous novel peptide. This peptide has an acute effect of enhancing calcium influx, thereby affecting meso-scale neuronal functioning in development, as well as a possible chronic role in Alzheimer's disease (Garcia-Rates S., Morrill P., Pottiez G., Badin A-S., Tormo-Garcia C., Heffner C. and Greenfield SA. (I) Pharmacological profiling of a novel modulator of the α7 nicotinic receptor: blockade of a toxic peptide increased in Alzheimer brain.). Hence, the present report and the companion study together provide novel evidence for the neurodegenerative process being an aberrant form of development: moreover, this trophic/toxic mechanism appears to be tractable to pharmaceutical intervention and as such, may open up the opportunity for innovative future therapy.

Author contributions

A-SB: responsible for data shown in Figs. 1–8 as well as the preparation of these same figures, plus MS preparation/writing. PM: responsible for data shown in Fig. 4A. ID: responsible for the data shown in Figs. 7 and 8 and preparation of Fig. 8. SAG: responsible for original basic concepts, planning overall programme, and assistance writing MS.

Author information and funding

SAG is a Senior Research Fellow, Lincoln College Oxford.

The authors declare competing financial interests. Susan Greenfield is the founder and CEO of Neuro-Bio Limited, a privately owned Company, and holds shares in the Company. Paul Morrill and Antoine-Scott Badin are employees of Neuro-Bio Ltd. Ian Devonshire is an employee of Nottingham University, seconded to Neuro-Bio Ltd. for four weeks. Correspondence and requests for materials should be addressed to Antoine-Scott Badin: scott.badin@neuro-bio.com.

Acknowledgements

The work described in this paper is covered by patent applications, WO 2015/004430 and GB1505239.2. We are very grateful to Professor Clive Coen (King's College London) for both editorial and scientific suggestions for the MS. We would also like to thank the following for their comments: Mr Charlie Morgan (Neuro-Bio Ltd), Professor John Stein (Oxford University). We are grateful to Dr Robin Murphy (Dept Psychology Oxford) for his help with the statistical analysis.

References

Andreollo, N.A., Santos, E.F., Araujo, M.R., Lopes, L.R., 2012. Rat's age versus human's age: what is the relationship? Arquivos brasileiros de cirurgia Dig. ABCD = Braz. Archives Dig. Surg. 25, 49–51.

Arendt, T., Bruckner, M.K., Lange, M., Bigl, V., 1992. Changes in acetylcholinesterase and butyrylcholinesterase in Alzheimer's disease resemble embryonic development–a study of molecular forms. Neurochem. Int. 21, 381–396.

Arendt, T., Bruckner, M.K., Bigl, V., Marcova, L., 1995. Dendritic reorganisation in the basal forebrain under degenerative conditions and its defects in Alzheimer's disease. II. Ageing, Korsakoff's disease, Parkinson's disease, and Alzheimer's disease. J. Comp. Neurol. 351, 189–222.

Auld, D.S., Kornecook, T.J., Bastianetto, S., Quirion, R., 2002. Alzheimer's disease and the basal forebrain cholinergic system: relations to beta-amyloid peptides, cognition, and treatment strategies. Prog. Neurobiol. 68, 209–245.

Badin, A.S., Eraifej, J., Greenfield, S., 2013. High-resolution spatio-temporal bioactivity of a novel peptide revealed by optical imaging in rat orbitofrontal cortex in vitro: possible implications for neurodegenerative diseases. Neuropharmacology 73, 10–18.

Berger, T., Borgdorff, A., Crochet, S., Neubauer, F.B., Lefort, S., Fauvet, B., Ferezou, I., Carleton, A., Luscher, H.R., Petersen, C.C., 2007. Combined voltage and calcium epifluorescence imaging in vitro and in vivo reveals subthreshold and suprathreshold dynamics of mouse barrel cortex. J. Neurophysiol. 97, 3751–3762.

Bon, C.L., Greenfield, S.A., 2003. Bioactivity of a peptide derived from acetylcholinesterase: electrophysiological characterization in guinea-pig hippocampus. Eur. J. Neurosci. 17, 1991–1995.

Bond, C.E., Zimmermann, M., Greenfield, S.A., 2009. Upregulation of alpha7 nicotinic receptors by acetylcholinesterase C-terminal peptides. PLoS One 4, e4846.

Bornstein, S.R., Ehrhart-Bornstein, M., Androutsellis-Theotokis, A., Eisenhofer, G., Vukicevic, V., Licinio, J., Wong, M.L., Calissano, P., Nistico, G., Preziosi, P., Levi-Montalcini, R., 2012. Chromaffin cells: the peripheral brain. Mol. Psychiatry 17, 354–358.

Bourgeois, E.B., Johnson, B.N., McCoy, A.J., Trippa, L., Cohen, A.S., Marsh, E.D., 2014. A toolbox for spatiotemporal analysis of voltage-sensitive dye imaging data in brain slices. PLoS One 9, e108686.

Broide, R.S., Leslie, F.M., 1999. The alpha7 nicotinic acetylcholine receptor in neuronal plasticity. Mol. Neurobiol. 20, 1–16.

Companion paper: Garcia-Rates S., Morrill P., Pottiez G., Badin A-S., Tormo-Garcia C., Heffner C. and Greenfield SA. (I) Pharmacological profiling of a novel modulator of the α7 nicotinic receptor: blockade of a toxic peptide increased in Alzheimer brain.

Coyle, J.T., Price, D.L., DeLong, M.R., 1983. Alzheimer's disease: a disorder of cortical cholinergic innervation. Sci. (New York, N. Y.) 219, 1184–1190.

Day, T., Greenfield, S.A., 2002. A non-cholinergic, trophic action of acetylcholinesterase on hippocampal neurones in vitro: molecular mechanisms. Neuroscience 111, 649–656.

Day, T., Greenfield, S.A., 2003. A peptide derived from acetylcholinesterase induces neuronal cell death: characterisation of possible mechanisms. Exp. Brain Res. 153, 334–342.

Day, T., Greenfield, S.A., 2004. Bioactivity of a peptide derived from acetylcholinesterase in hippocampal organotypic cultures. Exp. Brain Res. 155, 500–508.

Denk, W., Strickler, J.H., Webb, W.W., 1990. Two-photon laser scanning fluorescence microscopy. Sci. (New York, N. Y.) 248, 73–76.

Devonshire, I.M., Dommett, E.J., Grandy, T.H., Halliday, A.C., Greenfield, S.A., 2010. Environmental enrichment differentially modifies specific components of sensory-evoked activity in rat barrel cortex as revealed by simultaneous electrophysiological recordings and optical imaging in vivo. Neuroscience 170, 662–669.

Eimerl, S., Schramm, M., 1994. The quantity of calcium that appears to induce neuronal death. J. Neurochem. 62, 1223–1226.

Garcia-Rates, S., Lewis, M., Worrall, R., Greenfield, S., 2013. Additive toxicity of beta-amyloid by a novel bioactive peptide in vitro: possible implications for Alzheimer's disease. PLoS One 8, e54864.

Gerstein, G.L., Bedenbaugh, P., Aertsen, M.H., 1989. Neuronal assemblies. IEEE Trans. Bio-medical Eng. 36, 4–14.

Golomb, D., Wang, X.J., Rinzel, J., 1996. Propagation of spindle waves in a thalamic slice model. J. Neurophysiol. 75, 750–769.

Goodwin, D., Simerska, P., Toth, I., 2012. Peptides as therapeutics with enhanced bioactivity. Curr. Med. Chem. 19, 4451–4461.

Greenfield, S., 2013. Discovering and targeting the basic mechanism of neurodegeneration: the role of peptides from the C-terminus of acetylcholinesterase: non-hydrolytic effects of ache: the actions of peptides derived from the C-terminal and their relevance to neurodegeneration. Chem. Biol. Interact. 203, 543–546.

Greenfield, S.A., 2015. Neurological Disorders (UK).

Greenfield, S., Vaux, D.J., 2002. Parkinson's disease, Alzheimer's disease and motor neurone disease: identifying a common mechanism. Neuroscience 113, 485–492.

Greenfield, S.A., Day, T., Mann, E.O., Bermudez, I., 2004. A novel peptide modulates alpha7 nicotinic receptor responses: implications for a possible trophic-toxic mechanism within the brain. J. Neurochem. 90, 325–331.

Haworth, D., Rees, A., Alcock, P.J., Wood, L.J., Dutta, A.S., Gormley, J.J., Jones, H.B., Jamieson, A., Reilly, C.F., 1999. Anti-inflammatory activity of c(ILDV-NH(CH_2)5CO), a novel, selective, cyclic peptide inhibitor of VLA-4-mediated cell adhesion. Br. J. Pharmacol. 126, 1751–1760.

Hess, S., Linde, Y., Ovadia, O., Safrai, E., Shalev, D.E., Swed, A., Halbfinger, E., Lapidot, T., Winkler, I., Gabinet, Y., Faier, A., Yarden, D., Xiang, Z., Portillo, F.P., Haskell-Luevano, C., Gilon, C., Hoffman, A., 2008. Backbone cyclic peptidomimetic melanocortin-4 receptor agonist as a novel orally administrated drug lead for treating obesity. J. Med. Chem. 51, 1026–1034.

Kuhn, B., Denk, W., Bruno, R.M., 2008. In vivo two-photon voltage-sensitive dye imaging reveals top-down control of cortical layers 1 and 2 during wakefulness. Proc. Natl. Acad. Sci. U. S. A. 105, 7588–7593.

Loo, D.T., Copani, A., Pike, C.J., Whittemore, E.R., Walencewicz, A.J., Cotman, C.W.,

1993. Apoptosis is induced by beta-amyloid in cultured central nervous system neurons. Proc. Natl. Acad. Sci. U. S. A. 90, 7951–7955.
Mann, E.O., Greenfield, S.A., 2003. Novel modulatory mechanisms revealed by the sustained application of nicotine in the guinea-pig hippocampus in vitro. J. Physiol. 551, 539–550.
Nunez, J.L., Nelson, J., Pych, J.C., Kim, J.H., Juraska, J.M., 2000. Myelination in the splenium of the corpus callosum in adult male and female rats. Brain Res. Dev. Brain Res. 120, 87–90.
Paxinos, G., Watson, C., 1998. The Rat Brain. Elsevier, San Diego, USA.
Plant, T.D., Standen, N.B., 1981. Calcium current inactivation in identified neurones of Helix aspersa. J. Physiol. 321, 273–285.
Rossor, M.N., 1981. Parkinson's disease and Alzheimer's disease as disorders of the isodendritic core. Br. Med. J. 283, 1588–1590.
Saez-Valero, J., Sberna, G., McLean, C.A., Small, D.H., 1999. Molecular isoform distribution and glycosylation of acetylcholinesterase are altered in brain and cerebrospinal fluid of patients with Alzheimer's disease. J. Neurochem. 72, 1600–1608.
Senut, M.C., Menetrey, D., Lamour, Y., 1989. Cholinergic and peptidergic projections from the medial septum and the nucleus of the diagonal band of Broca to dorsal hippocampus, cingulate cortex and olfactory bulb: a combined wheatgerm agglutinin-apohorseradish peroxidase-gold immunohistochemical study. Neuroscience 30, 385–403.
Singer, W., 1993. Synchronization of cortical activity and its putative role in information processing and learning. Annu. Rev. Physiol. 55, 349–374.
Soreq, H., Seidman, S., 2001. Acetylcholinesterase–new roles for an old actor. Nat. Rev. Neurosci. 2, 294–302.
Sotty, F., Danik, M., Manseau, F., Laplante, F., Quirion, R., Williams, S., 2003. Distinct electrophysiological properties of glutamatergic, cholinergic and GABAergic rat septohippocampal neurons: novel implications for hippocampal rhythmicity. J. Physiol. 551, 927–943.
Tominaga, T., Tominaga, Y., Yamada, H., Matsumoto, G., Ichikawa, M., 2000. Quantification of optical signals with electrophysiological signals in neural activities of Di-4-ANEPPS stained rat hippocampal slices. J. Neurosci. Methods 102, 11–23.
Wang, S., Yao, Z., Wang, J., Ai, Y., Li, D., Zhang, Y., Mao, J., Gu, H., Ruan, Y., Mao, J., 2006. Evidence for a distinct group of nestin-immunoreactive neurons within the basal forebrain of adult rats. Neuroscience 142, 1209–1219.
Webb, C.P., Greenfield, S.A., 1992. Non-cholinergic effects of acetylcholinesterase in the substantia nigra: a possible role for an ATP-sensitive potassium channel. Exp. Brain Res. 89, 49–58.
Woolf, N.J., 1996. Global and serial neurons form A hierarchically arranged interface proposed to underlie memory and cognition. Neuroscience 74, 625–651.
Wu, J., Anwyl, R., Rowan, M.J., 1995. beta-Amyloid selectively augments NMDA receptor-mediated synaptic transmission in rat hippocampus. Neuroreport 6, 2409–2413.
Yuste, R., Tank, D.W., Kleinfeld, D., 1997. Functional study of the rat cortical microcircuitry with voltage-sensitive dye imaging of neocortical slices. Cereb. Cortex 7, 546–558.